Characterization of needle-assisted jet injections

Xinxin Li, Bryan Ruddy, Andrew Taberner

PII: S0168-3659(16)30953-1
DOI: doi: 10.1016/j.jconrel.2016.10.010
Reference: COREL 8501

To appear in: *Journal of Controlled Release*

Received date: 6 July 2016
Revised date: 3 October 2016
Accepted date: 11 October 2016

Please cite this article as: Xinxin Li, Bryan Ruddy, Andrew Taberner, Characterization of needle-assisted jet injections, *Journal of Controlled Release* (2016), doi: 10.1016/j.jconrel.2016.10.010

Title Page

Title: Characterization of Needle-assisted Jet Injections

Author names and affiliations:

Xinxin Li

Auckland Bioengineering Institute

The University of Auckland

Auckland, New Zealand

xli230@aucklanduni.ac.nz

Bryan Ruddy

Auckland Bioengineering Institute[1]

The University of Auckland

Auckland, New Zealand

Department of Engineering Science[2]

The University of Auckland

Auckland, New Zealand

b.ruddy@auckland.ac.nz

Andrew Taberner

Auckland Bioengineering Institute[1]

The University of Auckland

Auckland, New Zealand

Department of Engineering Science[2]

The University of Auckland

Auckland, New Zealand

a.taberner@auckland.ac.nz

Corresponding author:

Andrew Taberner

Auckland Bioengineering Institute[1]

The University of Auckland

Auckland, New Zealand

Department of Engineering Science[2]

The University of Auckland

Auckland, New Zealand

a.taberner@auckland.ac.nz

Present/permanent address:

Auckland Bioengineering Institute

The University of Auckland

Level 6, 70 Symonds St

Auckland 1024,

New Zealand

Abstract, Keywords & Abbreviations

Abstract:

Hypodermic injections have been the standard for transcutaneous drug delivery for many years. However, needle phobia, pain, and risks of needle-stick injuries have manifested in poor patient compliance. Needle-free jet injections (NFJI) have been developed to address these drawbacks but the reliability of dose and depth of delivery have been limited by a lack of control over jet parameters, and by variability in the skin's mechanical properties among individuals. Moreover, the device size and cost have been restrained by the high pressure (> 20 MPa) required to penetrate the skin. Needle-assisted jet injections have been proposed to improve delivery reliability of conventional jet injectors by penetrating the skin with a short needle (< 5 mm) and thereby allowing jet delivery to a desired injection depth at a reduced pressure.

This study characterised needle-assisted jet injections performed after first penetrating the skin with a 1.5 mm needle, examining the effect of needle size on jet parameters, and evaluating injection performance in porcine skin. A voice-coil actuated jet injector was modified to incorporate needles of 30 G, 31 G and 32 G. A series of pulse tests was performed to compare jet velocity and injection volume across the needle sizes, where it was found that the jet velocity and injection volume achieved with 32 G needles were 13 % and 16 % lower, respectively, than with 30 G. In contrast, there was no significant difference in jet velocity and injection volume between 30 G and 31 G needles, suggesting that a reduction of 10 μm in the mean inner diameter of the 31 G needle has minimal impact on jet velocity and injection volume.

Injection studies performed in porcine skin revealed that injections driven by fluid pressures ranging between 0.8 MPa and 1.4 MPa were able to achieve substantial injectate penetration (~10 mm) and delivery (~100 µL) into subcutaneous fat regardless of needle size, in a period of 40 ms. The required pressures are an order of magnitude lower than those used in NFJI, yet still maintain the high-speed nature of jet injection by achieving a delivery rate of 2.25 mL/s. The lower pressures required in needle-assisted drug delivery can lead to reduced device size and cost, as well as reduced shear stresses during jet injection and can therefore minimise the potentially adverse effect of shear on the structural integrity of proteins, vaccines and DNA.

Keywords:

Needle-assisted, Jet injection, Transdermal delivery, Voice coil

1. Introduction

Skin is recognised as one of the most effective routes for vaccine and drug delivery, offering both immunological and pharmacological advantages due to its multi-layered structure. Since the introduction of the needle and syringe in the mid-19th century, hypodermic injection has become the standard for cutaneous drug administration [1]. However, the pain, anxiety and needle phobia associated with needle injections have manifested in poor patient compliance among both children and adults [2]. Moreover, hypodermic injections are not limited to humans, but are also used in domestic animals such as cattle, sheep and chickens. Here, the use of hypodermic needles has presented difficulties in performing effective injections due to hair or fur, skin thickness, and cross contamination due to reuse of needles, thus resulting in considerable economic loss [3].

To address these drawbacks, alternative cutaneous delivery methods, including transdermal delivery systems and jet injectors, have been investigated. Transdermal patches, which often employ methods such as ultrasound, electroporation and microneedles to increase the permeability of skin, deliver drug molecules across the stratum corneum into the dermis. This delivery method is non-invasive and less painful compared to hypodermic injections, but is limited by a slow delivery rate and requires the use of hydrophobic molecules with low molecular weights [4]. In contrast, jet injection has the advantage of high speed delivery and can be applied to a wide range of liquid drugs including macromolecules. However, the reliability of most commercial spring powered jet injectors has been compromised by the lack of control of jet parameters and by skin variability among different body sites as well as between individuals [5, 6].

More recently, the idea of needle-assisted jet injection has been proposed as an alternative for improving the reliability and effectiveness of conventional jet injectors by first penetrating the skin with a short needle (typically < 5 mm) and delivering a fluid jet at high speed. With the needle already penetrating the toughest skin layer, such a system is able to achieve the desired injection depth at a reduced pressure, yet still maintains the high speed nature of jet injection with minimal pain. A lower pressure requirement leads to reduced device size and cost, as well as reduced shear stress during jet injection, thereby reducing the risk an damage to the structural integrity of proteins, vaccines and DNA [7]. Furthermore, factors that have been suggested to compromise jet injection performance such as hair or fur, variability in skin mechanical properties and movement during injection can be minimised by the combination of needle penetration and brief injection time [8].

Currently there is a lack of detailed analyses of injection performance in needle-assisted JI. Particularly absent is an analysis of the effect of jet parameters, needle size and length on penetration depth and injection volume. In addition, experimentation involving smaller needles (> 30 gauge) is also desirable for applications in humans, as shorter and thinner needles are less painful and therefore more likely to yield higher patient compliance. Based on these considerations, this paper evaluates the use of small needles in the range of 30 G to 32 G in needle-assisted jet injections through quantitative analysis of the effect of needle size on jet parameters and injection performance in post-mortem pig skin. The paper also investigates the relationship between fluid pressure and jet velocity developed within the injection system. This knowledge will facilitate the future design and development of needle-assisted jet injectors with better control over jet velocity and injection volume.

2. Materials and Methods

2.1. Device Development

Voice-coil injector

The jet injector used in this study (Figure 1) consisted of a custom-made linear voice-coil motor, a linear potentiometer used as a position sensor, a disposable piston and a custom-made stainless steel ampoule [9]. The total DC resistance of the coil was 9.4 Ω and the force constant over the used-stroke of the motor ranged between 9.0 $N \cdot A^{-1}$ and 10.2 $N \cdot A^{-1}$. The piston was attached to the front of the moving coil, with the potentiometer coupled to the edge in order to track the position of the voice-coil actuator. The ampoule head had a threaded compartment at the tip that could accommodate a stainless steel orifice that would typically be between 150 µm and 300 µm in diameter during a standard jet injection (Precision orifices type ZMNS-SS-V, O'Keefe controls Co.).

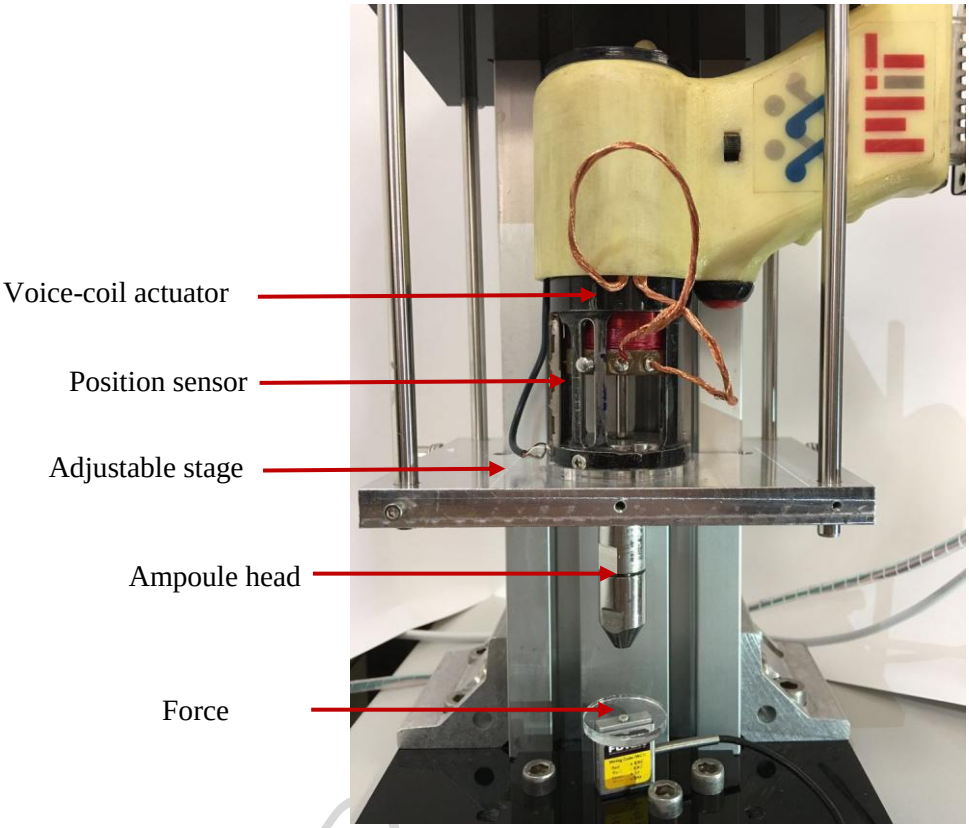

Figure 1: Needle-assisted jet injector experimental apparatus.

High speed monitoring and control of the coil position was achieved using a system comprising a real-time controller (cRIO-9024, National Instruments) embedded in a reconfigurable field-programmable gate-array (FPGA) chassis (cRIO-9113). The motor was driven by a linear power amplifier (AE Techron 7224), controlled by a PC-based data acquisition and control system running in National Instruments LabVIEW™ 11.1.

Tissue Force Measurement

The force applied by the injector to the tissue was measured with a small load cell (Futek, stock # FSH00104) with 44.5 N capacity fixed to the base of the vertical stand aligned with the needle. An acrylic plate was fixed on top of the sensor to avoid direct contact of fluid and the sensor (Figure 1). The sensor was connected to a bridge analog input module (NI 9237), and force data were sampled at 20 kHz, recorded by the FPGA "target" application at 10 kHz and filtered by a 10-point moving-average prior to display.

Needle-assisted jet injector

Three of the smallest needles that are commercially available were selected for this study. These were the BD Microlance™ 30 G needles, BD Micro-Fine™ 31 G pen needles and BD Micro-Fine™ 32 G pen needles respectively (Figure 2, A-C). 5 needles of each size were randomly selected and imaged using a SKYSCAN 1172 x-ray micro computed tomography (Micro-CT) machine to determine their outer and inner diameters (o.d. & i.d.). A comparison of the measured diameters and the nominal diameters provided in the Birmingham Wire Gauge Table is presented in Table 1.

Table 1 Comparison of needle diameters from Micro-CT measurements and the Birmingham Wire Gauge Table

Needle Size (G)	Nominal o.d. (mm)	Nominal i.d. (mm)	Measured o.d. (mm)	Measured i.d. (mm)
30	0.3112 ± 0.0064	0.159 ± 0.019	0.301 ± 0.008	0.157 ± 0.010
31	0.2604 ± 0.0064	0.133 ± 0.019	0.253 ± 0.010	0.147 ± 0.010
32	0.2096 ± 0.0064	0.108 ± 0.019	0.232 ± 0.009	0.126 ± 0.010

The needles were trimmed to a shorter length in order to minimise the resistance to flow as well as to ensure adequate penetration depth into the skin for effective injection. Laurent, et al. measured human skin thickness (epidermis and dermis) at different body sites and found the mean and 95 % confidence interval values of skin thickness across the deltoid, suprascapular region, waist, and thigh are greater than 1.5 mm regardless of gender, age (18-70 years old), ethnic origin and body mass index [10]. Based on these considerations, each needle was trimmed to 4 mm, inserted, and soldered into an orifice with 2 mm remaining above the orifice surface (Figure 2, D-F). The assembly of the needle-orifice to the jet injector is shown in Figure 3.

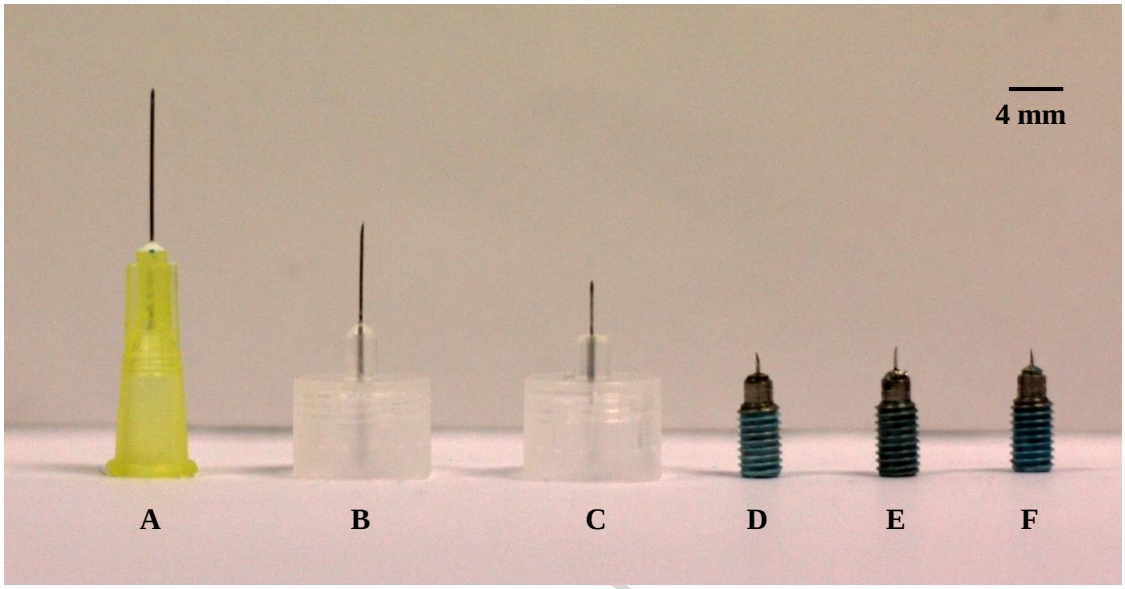

Figure 2: Needles prior to modification: (A) BD Microlance™ 30 G needle, 13 mm long (B) BD Micro-Fine™ 31 G pen needle, 8 mm long (C) BD Micro-Fine™ 32 G pen needles, 4 mm long. Needles are trimmed to 4 mm and soldered to the corresponding orifices with 2 mm length extending above the orifice: (D) 30 G needle fixed to a 300 µm orifice (E) 31 G needle fixed to a 260 µm orifice and (F) 32 G needle fixed to a 240 µm orifice.

Figure 3: Exploded view of the needle-assisted voice-coil actuated jet injector.

2.2Estimation of Jet Velocity

As voltage is applied to the voice coil actuator, the resulting current generates force to propel the piston forward and thereby accelerate fluid through the needle. Jet velocity can be estimated based on the conservation of volume, where the volume of fluid moved by the piston in the ampoule must equal the volume ejected through the needle, assuming there is no dead volume left within the injector system. By equating volumetric flow rates in the ampoule and needle, jet velocity can be obtained by

$$v_{jet} = \frac{r_{ampoule}^2}{r_{jet}^2} V_{piston}$$

where $r_{ampoule}$ is the radius of the ampoule shaft, r_{jet} is the radius of the jet as it exits the needle tip and V_{piston} is the piston velocity measured in m·s^{-1}. High speed video (Phantom Micro LC 110 camera) of the fluid jet revealed the cylindrical shape of the fluid jet as it exits the needle tip and that the jet diameter closely matches the i.d. of the needle (Figure 4). Therefore the inner radius of the needle can be used as an approximation of r_{jet}. The piston position, measured in millimetres, was proportional to the corresponding volume, where 1 mm of piston movement along the ampoule shaft ejects 10 µL of fluid. Figure 5B shows the piston position during an injection test (a "pulse test") directed at the load-cell, where 52 V is applied to the actuator for 40 ms. As shown in Figure 5A, a current of 5.5 A is induced, generating approximately 48 N of coil-force at steady state between 20 ms and 40 ms. The voice-coil accelerates the piston and fluid for a period of 10 ms; fluid impacts the load-cell approximately 10 ms after the start of the test. The steady state piston velocity is quantified from the slope of the piston position trace during this time period and the total ejected volume during an injection is determined from the difference between the final and initial piston position.

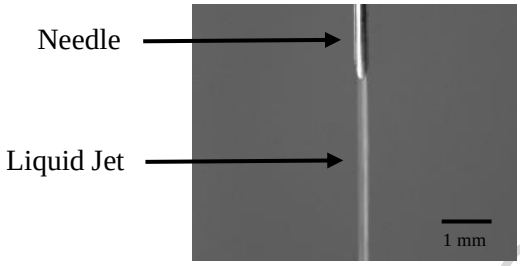

Figure 4: Photograph of the fluid jet as it exits the needle during a pulse test.

2.3Effect of Needle Size on Jet Parameters

Statistical Analysis

The effect of needle size was examined by comparing the jet velocity and injection volume when a fixed voltage of 52 V was applied over 40 ms and jets were created from 30 G, 31 G and 32 G needles. For each needle size, six needles were selected randomly and each was subjected to four injections. This gave rise to 24 injections per needle size and a total of 72 injections.

Single factor ANOVA with repeated measures analyses were then performed in the *R* statistics package (the University of Auckland, New Zealand) to examine the effect of needle size on jet velocity as well as injection volume, where needle size was the factor of interest and the needles tested within each needle size group were the repeated measures.

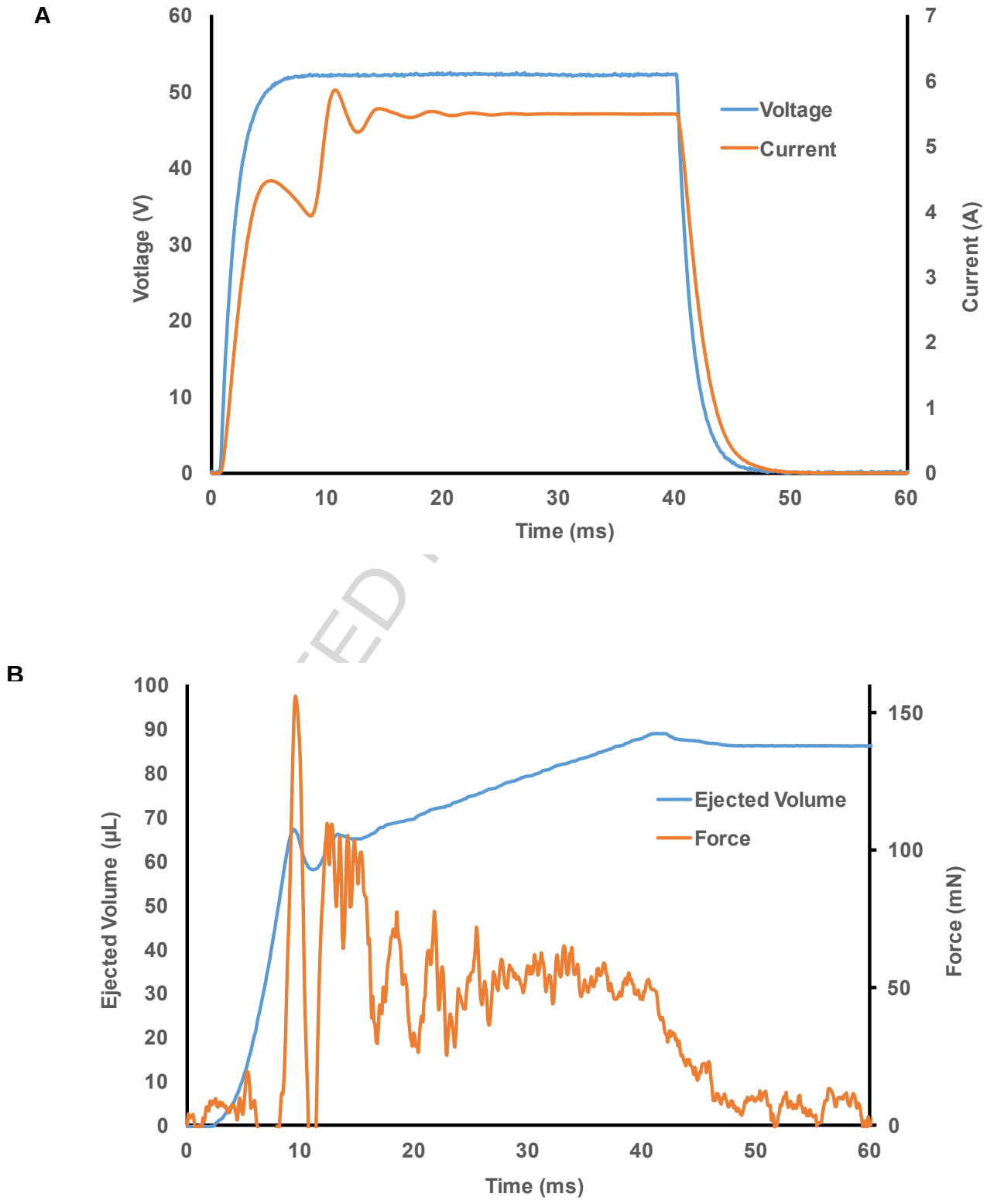

Figure 5: Pulse test of 31 G needle; 52 V is applied for 40 ms. (A) Applied voltage and induced current during the pulse test. (B) Recorded piston position and jet force.

Pulse tests

The jet velocity vs. voltage profile was obtained for each needle size by performing tests with incremental changes in applied voltage. For each needle size, three needles were selected randomly, mounted into the JI and each subjected to five injections with voltage ranging from 24 V to 72 V in 14 V increments applied over 40 ms. A total of 45 injections (15 × 3) were performed. The mean jet velocity and mean injection volume were calculated for each needle size and plotted against applied voltage.

2.4Polyacrylamide gel injections

Polyacrylamide gels have been used as models of soft tissues in many studies, as they can be formulated with Young's moduli that fall within the range of measured modulus values for human skin. The gel also offers the advantage of transparency, and therefore allows the penetration depth and injection pattern to be easily compared across different needle sizes.

Gel preparation

Polyacrylamide gels were prepared by diluting acrylamide solution (30% Acrylamide/Bis solution, 37.5:1, Bio-Rad Laboratories) with deionised water to obtain an acrylamide concentration of 10 %. The diluted solution was then polymerised by the addition of 10 % ammonium persulfate and N, N, N`, N`-tetramethylethylenediamine to the ratio of 3300:3:5. The mixed solution was poured into cylindrical clear polystyrene containers (diameter = 26 mm, height = 26 mm) and allowed to set in a fume hood overnight.

Injection protocol

Injections were performed into three gel samples for each needle size. Water and food colouring concentrate (Queen Food Colour Blue, 50 mL) was mixed in a ratio of 10:1 and used as injectate for visualisation purposes. During an injection, the gel was placed on top of the force transducer with the centre of the container aligned with the needle. The injector was then lowered by adjusting the vertical stage until the entire length of the needle (~1.5 mm) had penetrated the gel and a contact force of 0.8 N had been reached. A pulse test was then performed with 52 V applied over 40 ms. The injected sample was immediately photographed after the injection to capture the injectate penetration and dispersion pattern.

2.5Porcine Skin Injections

Porcine skin is a preferred in vitro model for human skin in studies on percutaneous absorption. Porcine tissue shares many similarities with human skin in terms of skin thickness, collagen arrangement and vascular anatomy in the dermis as well as the contents of stratum corneum [11, 12]. By visualising injectate penetration in porcine skin using x-ray micro computed tomography (Micro CT), the injectate dispersion in different skin layers can be obtained and analysed through image reconstruction and segmentation.

Tissue Preparation

Porcine tissue was obtained, post-morterm, from pigs aged between ten to twelve weeks, in accordance with the University Of Auckland Code Of Ethical Conduct for the Use of Animals for Teaching and Research. Skin with two layers of muscle was harvested from the torso region of the pig within two hours of euthanasia. The skin samples were then vacuum sealed and stored at –80 ºC for later use (for no longer than six months). In this study, torso skin specimens from three pigs were used to prepare a total of fifteen samples.

Prior to experimentation, the tissue was allowed to defrost at room temperature for at least six hours and then cut into cylindrical samples by following the edge of the plastic container described in section 2.4 with a scalpel. The skin samples had diameters of approximately 25 mm and heights ranging from 17.50 mm to 20 mm depending on the actual skin thickness. The mass of each sample was measured prior to injection.

Micro-CT Contrast Solution Preparation

An iodine-based CT contrast solution (Omnipaque^{TM} 300 mg·ml^{-1}, GE Healthcare) was used to allow visualisation of the injectate in Micro-CT scans. The injectate solution was prepared by mixing the contrast solution with deionised water and food colouring in a ratio of 15:35:1 by volume.

Injection Protocol

In a manner similar to gel experiments, a tissue sample was placed on top of the force transducer with the centre of the tissue aligning with the needle. The injector was then lowered until the entire length of the needle had penetrated the tissue and a contact force of 0.8 N had been reached. The injection was performed using a pulse test with 52 V applied over 40 ms. The needle insertion point was marked upon removal of the needle and the post-injection weight was also measured. The tissue was then immediately transferred to the -80 °C freezer and stored for 15 minutes to minimise injectate diffusion after the injection and during the Micro-CT scanning process.

Micro-CT Scan and Image Reconstruction

Each frozen tissue sample was scanned using the Micro-CT scanner at 12 µm voxel size over scanning time of approximately one hour and thirty minutes. Image reconstruction was performed using the NRecon software (Bruker microCT, Belgium). Segmentation of different tissue layers (epidermis + dermis,

subcutaneous fat and muscle) was then performed in the CT-An software (Bruker microCT, Belgium). The injectate was also segmented out from the surrounding tissue and stored as a series of bitmap images at different depths from the surface, where each image contained pixel intensity values for further analysis in Matlab. The injection point was identified on the image where the injectate first appeared, counting from the skin surface downwards, and the bottom of the bolus as the first image after injectate had disappeared. The distance between these two images was defined as the penetration depth. The percentage of injectate in each tissue layer as well as the centre of mass of the bolus was determined using code written in Matlab. The 3-D injectate bolus was visualised in the CT-Vox software (Bruker microCT, Belgium).

3. Results and Discussion

3.1 Effect of Needle Size on Jet Parameters

Statistical Analysis

Results from the ANOVA tests show that, at the 95 % confidence interval, there is a statistically significant difference in the mean jet velocities achieved from the three different needle sizes (p-value = 0.0292 < 0.05). For injection volume, the p-value is 0.083, suggesting there is no significant relationship between mean injection volume and needle size.

Pairwise comparisons were then performed to identify the source of the difference. As shown in Table 2, significant differences in jet velocity are found between 30 G and 32 G as well as between 31 G and 32 G. The mean jet velocity for 32 G needles is 13 % and 10 % lower than 30 G and 31 G respectively (Table 4). In Table 3, a significant difference in injection volume is also found between 30 G and 32 G needles, where a 16 % decrease in mean

injection volume was observed. Although Table 4 demonstrates a 6 % mean volume reduction between 31 G and 32 G needles, both groups exhibit relatively large standard deviations resulting in overlapping ranges of injection volumes.

Table 2 P-values from pairwise comparisons of jet velocity using single factor ANOVA with repeated measures

	30 G	**31 G**
31 G	0.512	-
32 G	0.0109	0.065

Table 3 P-values from pairwise comparison of injection volume using single factor ANOVA with repeated measures

	30 G	**31 G**
31 G	0.122	-
32 G	0.0257	0.526

Table 4 Mean jet velocity and injection volume with standard error (SE) of three different needle sizes obtained from pulse tests with 52 V voltage applied over 40 ms

Needle Size	Jet Velocity ($m \cdot s^{-1}$)	Injection Volume (µl)
30 G	50.25 ± 0.71	110.8 ± 1.9
31 G	48.68 ± 0.96	98.3 ± 3.1
32 G	43.71 ± 0.87	92.6 ± 3

Pulse Response

Figure 6A shows the relationship between applied voltage and velocity of the needle-assisted JI for the three different needle sizes. The overlapping traces of the 30 G and 31 G needles imply that a reduction of approximately 10 µm in needle i.d. has minimal impact on jet velocity, with only about 5 % reduction in jet velocity at 48 V, 60 V and 72 V. The Micro CT scans of the needles in Table 1 shows a large overlap of the distributions of the diameters for these two gauges, and therefore it is likely that some of the 31 G needles tested may actually fall within the 30 G diameter range. In contrast, the 32 G needle has a smaller increase in jet velocity with incremental applied voltage, suggesting that a 30 µm decrease in needle i.d. has resulted in significantly more resistance to flow. The amount of reduction in jet velocity between 30 G and 32 G needles also appears to increase with higher voltage.

This is depicted in Table 5 as an 18 % jet velocity reduction at 36 V compared to 23 % at 60 V. A similar trend is also observed in Figure 6B, where the volume difference is more significant between 30 G and 32 G needles compared to that between 30 G and 31 G needles. As shown in Table 6, a 10 % average reduction in volume was observed across all voltage levels as needle size decreases from 30 G (mean i.d. = 157 µm) to 32 G (mean i.d. = 126 µm).

Table 5 Mean jet velocity ($m \cdot s^{-1}$) with standard error (SE) of needles with incremental change in applied voltage from 24 V to 72 V

Needle size	24 V	36 V	48 V	60 V	72 V
30 G	27.06 ± 0.48	36.75 ± 0.97	48.42 ± 0.33	56.37 ± 0.21	63.16 ± 0.40
31 G	29.67 ± 0.32	40.31 ± 0.12	47.62 ± 0.19	53.66 ± 0.24	60.19 ± 0.24
32 G	23.83 ±0.62	30.45 ± 0.84	38.4 ± 0.29	43.16 ± 0.33	50.21 ± 0.54

Table 6 Mean injection volume (µl) with standard error (SE) of needles with incremental change in applied voltage from 24 V to 72 V

Needle size	24 V	36 V	48 V	60 V	72 V
30 G	85.2 ± 2.3	88.0 ± 1.5	100.1 ± 0.5	103.1 ± 1.7	110.8 ± 0.4
31 G	86.0 ± 1.5	87.8 ± 0.5	91.9 ± 0.9	99.4 ± 1.5	100.8 ± 1.9
32 G	70.6 ±0.4	82.6 ± 2.2	84.6 ± 1.4	93.4 ± 1.0	96.8 ± 0.2

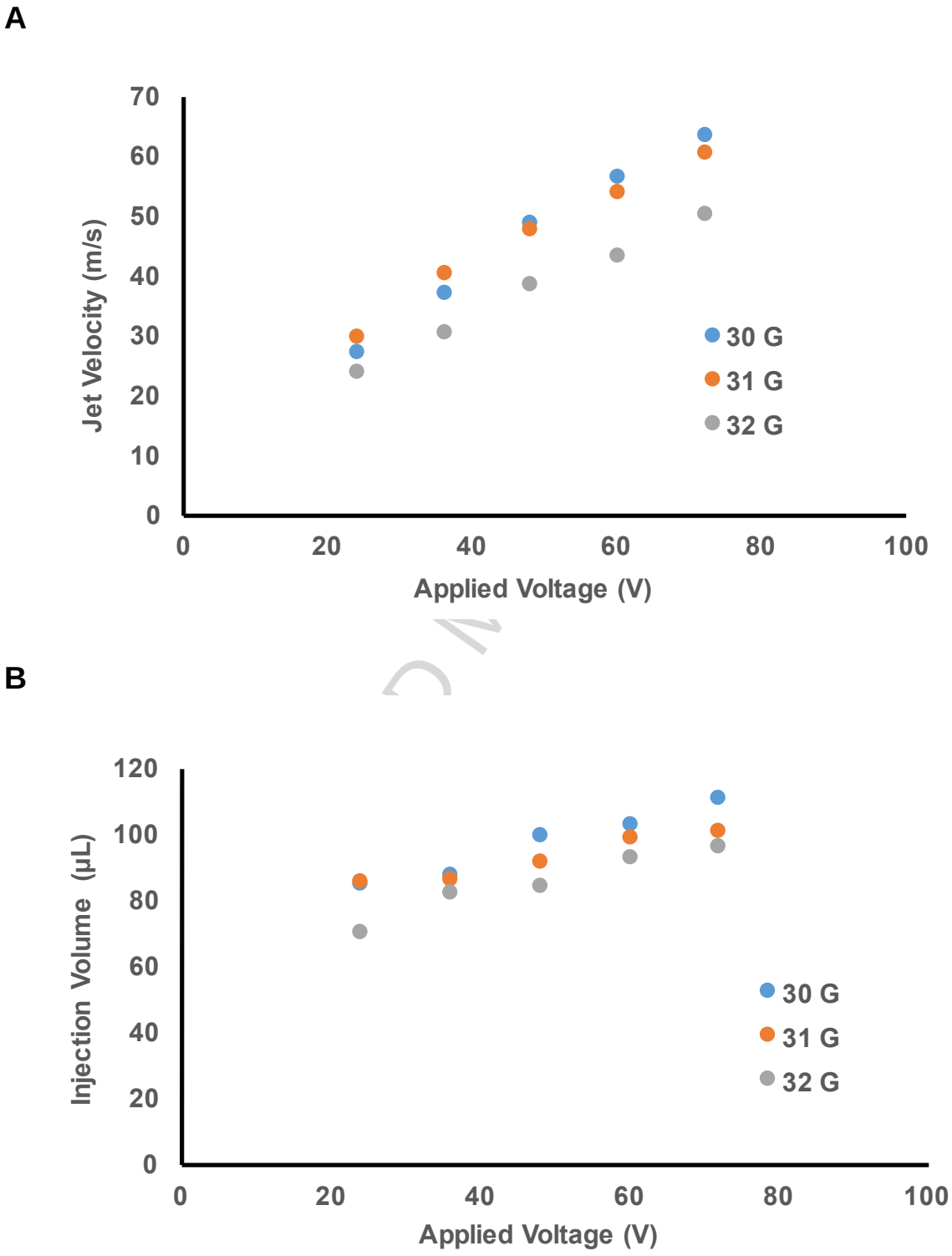

Figure 6: Results from sharp pulse tests with incremental change in voltage from 24 V to 72 V for 30 G, 31 G and 32 G needles. (A) Volumetric jet velocity vs. applied voltage (B) Injection volume vs. applied voltage.

3.2 Injectate Dispersion in Polyacrylamide Gel

A typical injectate bolus in polyacrylamide gel is shown in Figure 7. The width of the bolus was measured to quantify injectate dispersion in the radial direction. The penetration depth was defined as the distance between the position of the needle tip (dotted line) and the bottom of the bolus (solid line), and the injection volume was estimated from the piston trajectory. In all injections the bolus shape was similar to those observed in needle-free injections, where the width was slightly longer than the dispersion depth [13]. In needle-free injections an injection channel is formed and penetrates into the gel until a stagnation point is reached. Drug dispersion centres about the stagnation point and resembles a circular shape. However in needle-assisted jet injections, needle insertion would have already created a weak point for the fluid to propagate into and therefore there was no distinct injection channel. As shown in the side and top views in Figure 7, the injection created a two dimensional fracture plane represented by the darker blue region. Dispersion of fluid, represented by the lighter blue region, was evenly distributed around the plane. The shape of the bolus was also unsymmetrical around the injection point. In the front view of Figure 7, the injectate on the right was higher in position than the left. This was due to the fact that the needles have angled tips, resulting in fluid being pushed out over a shallower area on the side of the opening of the needle tip.

Mean injection volume, penetration depth, and injectate width of injections performed using the three different needle sizes are compared in Table 7. The mean injection volume decreased by 5.0 % and 16.0 % for 31 G and 32 G needles, respectively, when compared to 30 G needles. Reduction in volume also corresponded to decrease in injection depth, where 11.1 % and 17.0 % reduction in injection depth were observed in 31 G and 32 G respectively. On the other hand injection width increased with decreasing needle diameter,

suggesting that lower fluid pressures and jet velocities result in shallower and wider injectate dispersion.

Table 7 Results from gel injections showing mean injection volumes, penetration depths and widths of the injectate boluses for three different needle sizes. Standard errors were obtained from 5 tissue samples for each needle size

Needle size	Injection Volume (µL)	Injection Depth (mm)	Injection Width (mm)
30 G	96.7 ± 2.2	11.25 ± 0.43	3.45 ± 0.17
31 G	91.9 ± 0.9	10.00 ± 0.58	3.17 ± 0.17
32 G	81.2 ± 3	9.33 ± 0.17	3.23 ± 0.15

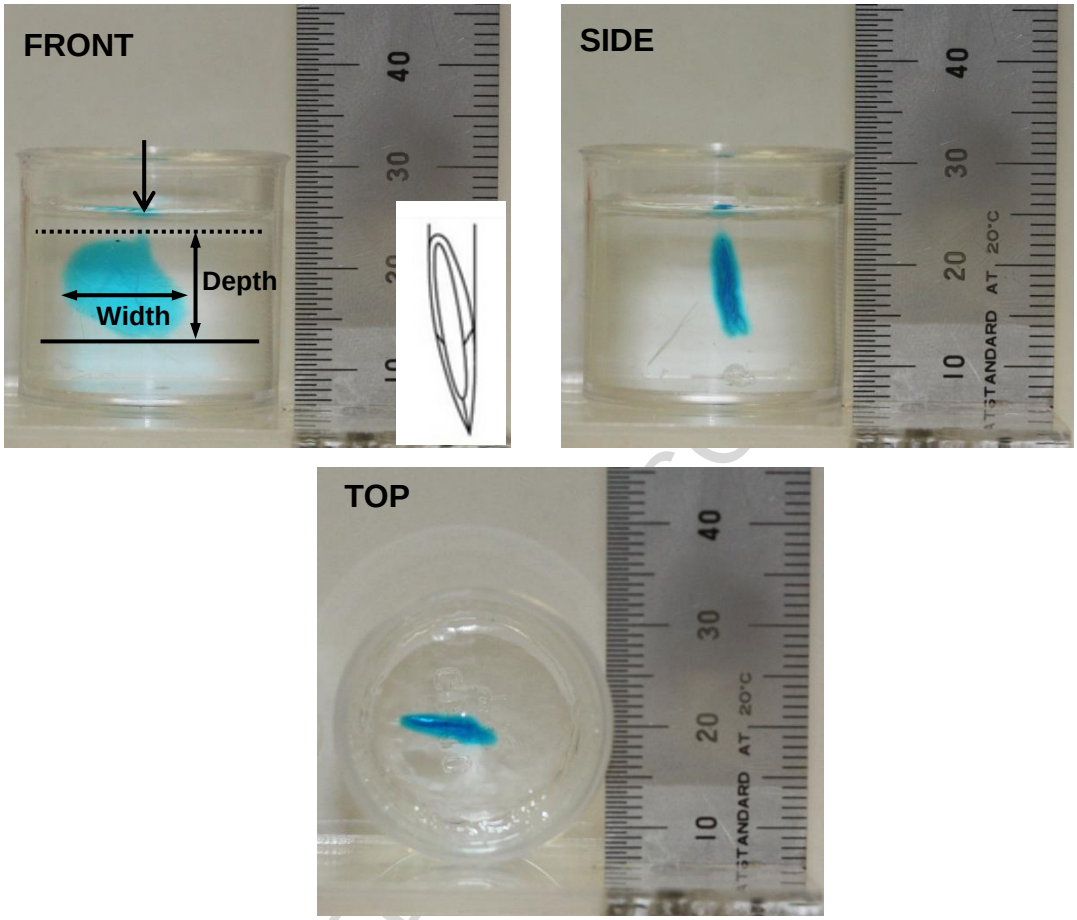

Figure 7: Injection into gel using a 30 G needle. The black dotted line represents the starting point of the injection (i.e. tip of needle) and the distance between the dotted and solid black lines is the penetration depth. The width of the bolus was measured as the maximum length of the bolus in the radial direction.

3.3 Injection Performance in Porcine Skin

Injection Volume

The change in tissue sample weight before and after the injection was used to infer the delivered volume by assuming a density of 1000 $kg \cdot m^{-3}$. The delivered volumes were then compared across different needle sizes using an ANOVA test; the resultant p-value was 0.639, suggesting there was no significant difference in the injected volume across different needle sizes. For each needle size, the weighed volume from tissue experiments was also compared with the mean volume obtained from same injection performed in air. In all needle size groups the volumes injected into tissues were less than their air injection counterparts (**Error! Reference source not found.**Figure 8). For 30 G needles, the volume injected into tissue was 22.3 % less than in air. For 31 G and 32 G needles, the reduction in volume was 12.2 % and 15.6 % respectively.

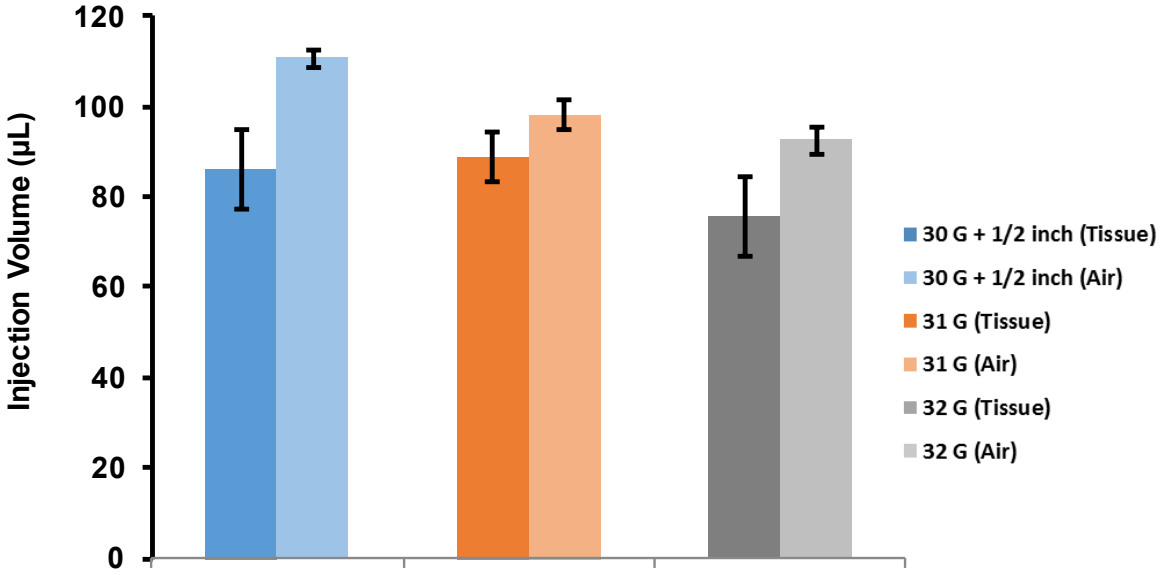

Figure 8: Mean injection volumes into tissue and into air.

Jet Velocity

A reduction in jet velocity was also observed in tissue experiments for all needle sizes when compared to the air injection counterparts (Figure 9). The mean jet velocity in tissue was decreased by 8.0 %, 2.3 % and 6.1 % for 30 G, 31 G and 32 G needles respectively. ANOVA analysis comparing jet velocities across different needle size groups suggested significant difference in jet velocities among the three groups. Pairwise ANOVA comparisons revealed significant difference in jet velocities between 30 G and 32 G, as well as between 31 G and 32 G needles. This implied that the effect of needle size on jet velocity was the same in both air and tissue experiments.

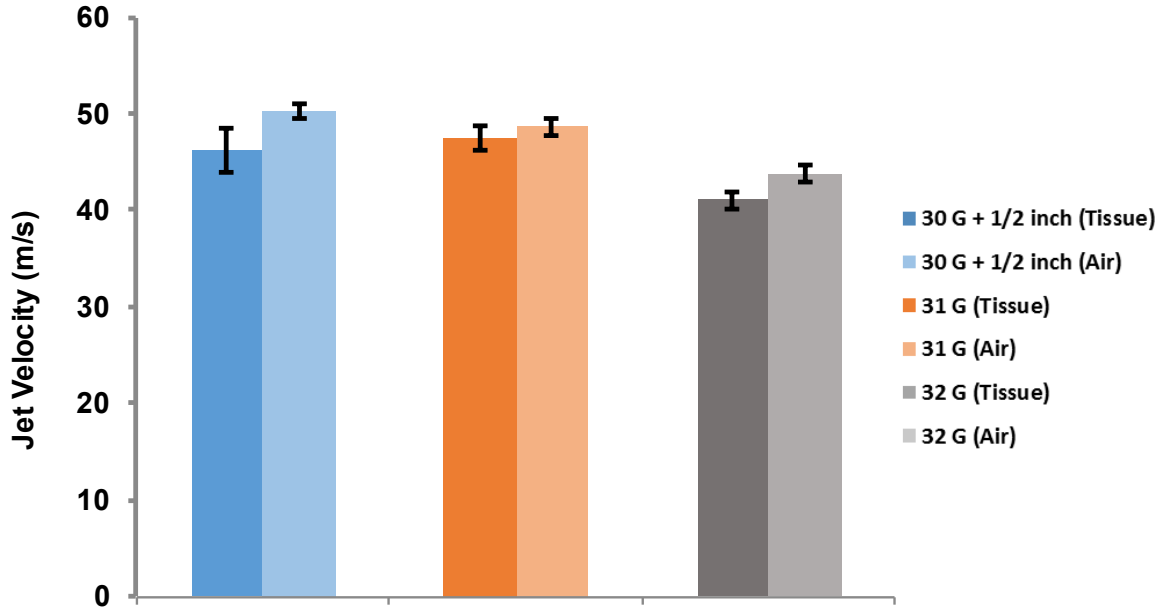

Figure 9: Mean volumetric jet velocities during injections into tissue and into air.

Injectate Dispersion

Penetration depth was determined by manually finding the injection point and the bottom of the injectate bolus in the segmented microCT images. As shown in Table 8, all three needle sizes have overlapping injection depths, suggesting there was no significant difference in penetration depth across the three needle sizes. Segmentation of the three skin layers demonstrated that in general, the injection started near the end of the dermis layer, with an average of over 64 % of the injectate delivered to the subcutaneous fat. In some tissue samples, where the fat layers were thinner, a small proportion of the injectate had reached the muscle layer. The averaged percentage of injectate delivered to each of the three layers is summarised in Table 9.

Table 8 Mean Injection Depth (with standard error) in tissue experiments

Needle size	Injection Depth (mm)
30 G	9.01 ± 1.05
31 G	9.21 ± 1.39
32 G	9.33 ± 0.70

Table 9 Averaged percentage of injectate (with standard error) delivered to each of the three skin layers

Needle Size	Percentage of Injectate (%)		
	Dermis	**Subcutaneous fat**	**Muscle**
30 G	2.80 ± 0.81	64.09 ± 13.95	33.11 ± 14.12
31 G	1.29 ± 0.66	70.85 ± 17.43	27.86 ± 17.15
32 G	5.02 ± 2.10	76.90 ± 12.62	18.09 ± 12.15

The 3-D coordinates of the centre of mass (CoM) of each bolus were also determined from the segmented images. In all cases the CoM was found to deviate from the injection points on the horizontal plane, suggesting that jet penetration was deviated by the inhomogeneous tissue structure. Ten out of the fifteen injections had over 90% of the injectate delivered to the subcutaneous fat and similar elliptical boluses were observed in these tissue samples (Figure 10), except for one sample where the jet penetrated perpendicularly into the tissue by 6 mm before dispersing into an elliptical shape (Figure 11).

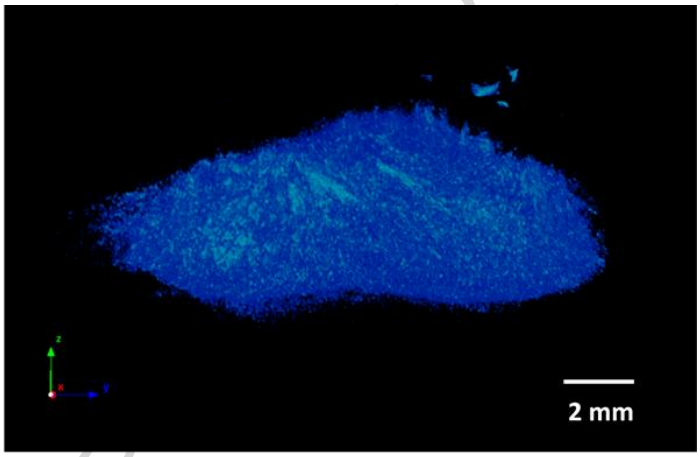

Figure 10: Elliptical dispersion patterns of injectate within subcutaneous fat in an injection with 31 G needle.

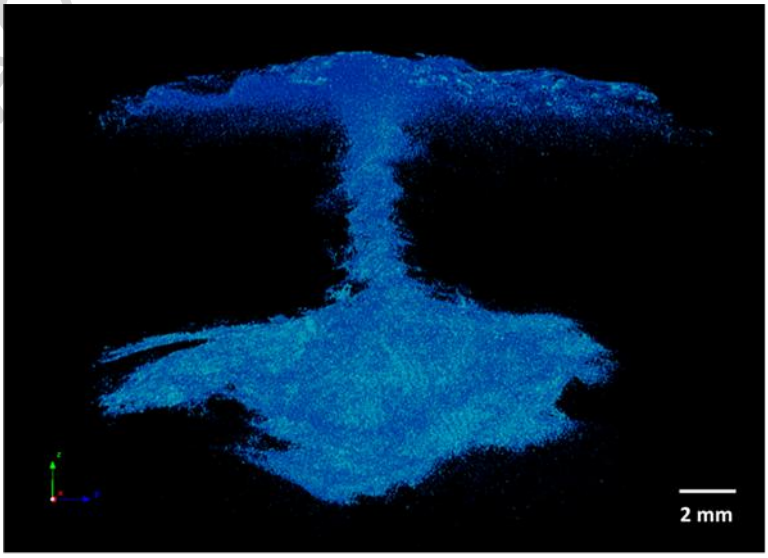

Figure 11: Perpendicular jet penetration followed by elliptical dispersion of injectate in subcutaneous fat.

Segmented images of injectate dispersion revealed the sponge-like dispersion pattern in subcutaneous fat, similar to those reported in previous literatures for subcutaneous injections with 27 G needles at a much lower syringe plunger speed of 2.90 $mm \cdot s^{-1}$ and with 21 G needles at 0.1 $mm \cdot s^{-1}$ [14, 15]. As shown in Figure 12, the thin bright lines running throughout the bolus represent the micro-channels created by the force of the jet. The injectate flowed through these channels and diffused into surrounding tissue. The formation of these micro-channels has been suggested to occur along the collagen septa surrounding lobules of adipocytes with relatively lower strength compared to the adipose tissue as a whole. By injecting pressurised fluid at high speed more micro-channels were formed, which increased the overall permeability of the subcutaneous tissue [15].

In another two injections, where the subcutaneous fat layer was thinner (< 4 mm) compared to other tissue samples, over 90 % of the injectate was delivered into the muscle layer. In both cases the dispersion shapes were long and thin which could be related to the parallel arrangements of the muscle fibres (Figure 13).

Our results showed that injectate dispersion is significantly affected by the multi-layered structure and inhomogeneous material properties of the skin. Skin thickness and mechanical properties are highly variable across different body sites within as well as between individuals, further complicating evaluations of injection performance. Both injection volume and jet velocity were reduced in tissue injections compared to injections into air due to the skin's mechanical strength acting against the pressurised fluid. At the voltage level tested in this study, with roughly 50 N of steady state force provided to the injector, there were no significant differences in penetration depth and injection volume observed in tissue between the three different needles sizes, suggesting that the use of the thinner 32 G needles could be more favourable for reducing pain without compromising injection performance. Furthermore, in our study, the

applied voltage during the tissue injection was able to generate jets with fluid pressures between 0.8 MPa to 1.4 MPa, with all tissue injections demonstrating substantial injectate penetration into subcutaneous fat. These pressures are an order of magnitude lower than those used in needle-free jet injection, suggesting that needle-assisted jet injection can potentially utilise a smaller motor and hence reduce the overall device size.

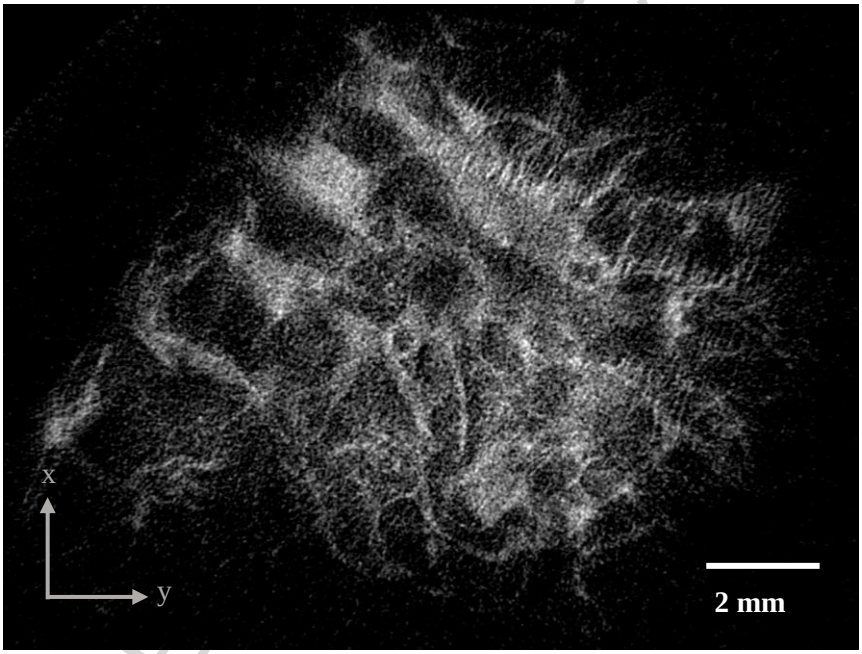

Figure 12: Segmented image of injectate dispersion in subcutaneous fat.

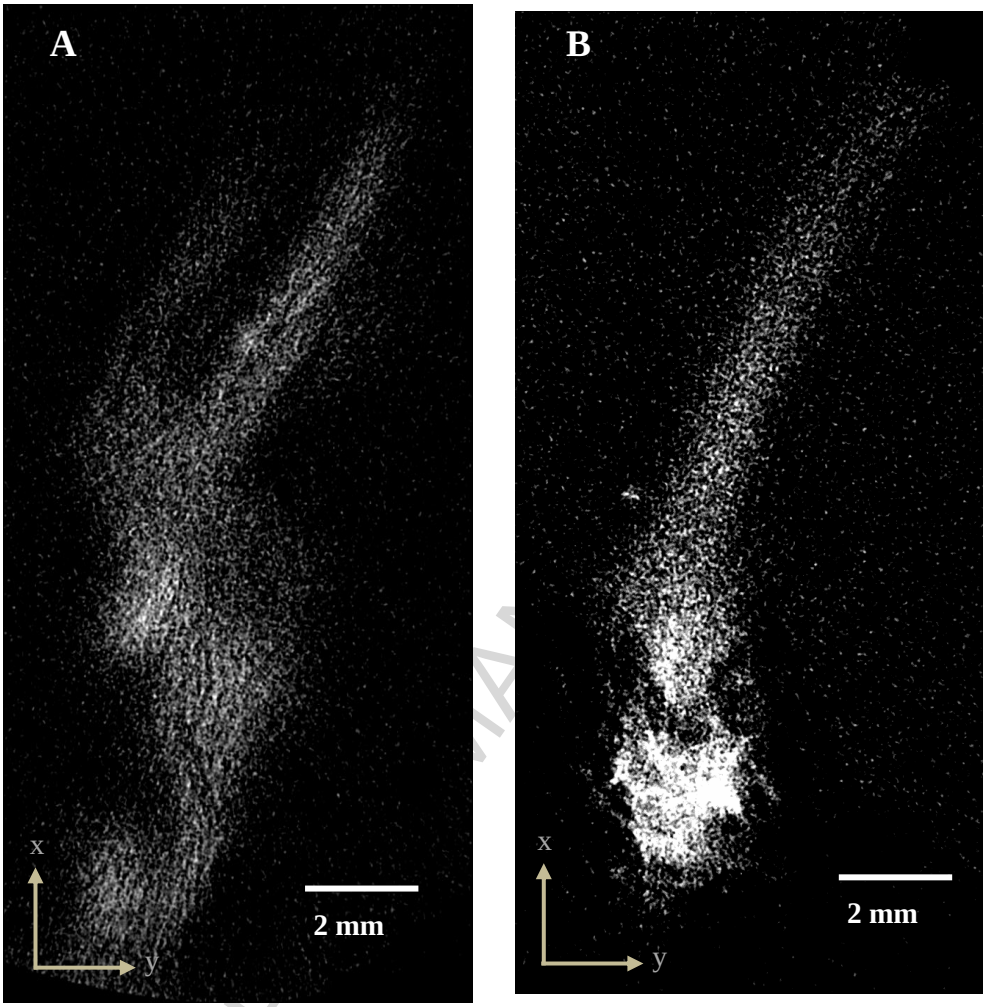

Figure 13: Segmented image of injectate dispersion from two injections into muscle.

4. Conclusion

This study has provided a quantitative analysis of needle-assisted jet injections by examining the effect of needle size on jet parameters and injection performance in tissue. Injection tests with incremental applied voltages on 30 G, 31 G and 32 G needles showed no significant difference in jet velocity and injection volume between 30 G and 31 G needles, suggesting that a reduction of 10 μm in the mean i.d. of the 31 G needle has minimal impact on jet velocity and injection volume. On the other hand, a 30 μm decrease in i.d. from 30 G to 32 G increased the resistance to flow significantly, resulting in 13 % reduction in mean jet velocity and 16 % reduction in injection volume.

The effect of needle size on injection performance in polyacrylamide gel and porcine tissue has also been examined. While injections into polyacrylamide gels demonstrated a positive correlation between penetration depth and needle size, this was not the case in porcine tissue. Both the jet velocity and injection volume decreased in tissue experiments compared to the previous tests performed in air. Moreover, there were no significant differences found in penetration depth and injection volume between the three needle sizes, suggesting that the 32 G needles could be used to reduce pain without compromising injection performance. With the needle already penetrated 1.5 mm into the dermis, it was found that injections driven by fluid pressures ranging between 0.8 MPa to 1.4 MPa were able to achieve injectate penetration of up to 9 mm, and delivery volumes of up to 90 μL into subcutaneous fat, regardless of needle size, within a period of 40 ms. This amounts to a volumetric flow rate of 2.25 mL/s; there is no reason why higher volumes of drug could not be delivered by extending the period of pressure application, although this was not attempted.

These pressures are an order of magnitude lower than those used in needle-free jet injection, suggesting that needle-assisted jet injection may offer many of the advantages of needle-free jet injection (controllability, diminished risk of needle-stick injury, lowered pain) while avoiding the need to develop the very high jet pressures required to first penetrate through the dermis. Furthermore, the lower pressure requirement leads to reduced device (motor) size and cost, as well as reduced shear stresses during jet injection thereby diminishing the possible adverse effect of shear stress on the structural integrity of proteins, vaccines and DNA during delivery. After implementing real-time feedback control of fluid volume and speed, we expect to achieve similar or better control as has previously been demonstrated in servo controlled needle-free jet injection [9]. In this way, we anticipate being able to deposit the injectate to any desired depth between 1.5 mm and 9 mm under the skin, potentially avoiding the stimulation of pain receptors.

Funding

This work was supported by the Medical Technologies Centre of Research Excellence (MedTech CoRE), funded by the Tertiary Education Commission of New Zealand.

REFERENCES

[1] B. G. Weniger and M. J. Papania, "Alternative vaccine delivery methods," *Vaccines, 5th ed. Amsterdam: Elsevier,* pp. 1357-92, 2008.

[2] H. S. Gill and M. R. Prausnitz, "Does needle size matter?," *Journal of diabetes science and technology,* vol. 1, pp. 725-729, 2007.

[3] D'antonio, Nicholas F., Nicholas J. D'antonio, and Richard O. Colvin. "Hypodermic injection system." U.S. Patent No. 8,864,713. 21 Oct. 2014.

[4] M. R. Prausnitz, S. Mitragotri, and R. Langer, "Current status and future potential of transdermal drug delivery," *Nature Reviews Drug Discovery,* vol. 3, pp. 115-124, 2004.

[5] S. Mitragotri, "Current status and future prospects of needle-free liquid jet injectors," *Nature Reviews Drug Discovery,* vol. 5, pp. 543-548, 2006.

[6] N. C. Hogan, A. J. Taberner, L. A. Jones, and I. W. Hunter, "Needle-free delivery of macromolecules through the skin using controllable jet injectors," *Expert Opinion on Drug Delivery,* vol. 12, pp. 1637-1648, 2015.

[7] Sadowski, Peter L., et al. "Needle assisted jet injector." U.S. Patent No. 7,776,015. 17 Aug. 2010.

[8] D'antonio, Nicholas F., Linda F. D'antonio, and John T. Wagner. "Hypodermic fluid dispenser." U.S. Patent No. 6,056,716. 2 May 2000.

[9] A. Taberner, N. C. Hogan, and I. W. Hunter, "Needle-free jet injection using real-time controlled linear Lorentz-force actuators," *Medical Engineering and Physics,* vol. 34, pp. 1228-1235.

[10] A. Laurent, F. Mistretta, D. Bottigioli, K. Dahel, C. Goujon, J. F. Nicolas, *et al.*, "Echographic measurement of skin thickness in adults by high frequency ultrasound to assess the appropriate microneedle length for intradermal delivery of vaccines," *Vaccine,* vol. 25, pp. 6423-6430, 2007.

[11] I. P. Dick and R. C. Scott, "Pig ear skin as an in‐vitro model for human skin permeability," *Journal of Pharmacy and Pharmacology*, vol. 44, pp. 640-645, 1992.

[12] B. Godin and E. Touitou, "Transdermal skin delivery: predictions for humans from in vivo, ex vivo and animal models," *Advanced drug delivery reviews*, vol. 59, pp. 1152-1161, 2007.

[13] J. Schramm-Baxter and S. Mitragotri, "Needle-free jet injections: dependence of jet penetration and dispersion in the skin on jet power," *Journal of Controlled Release*, vol. 97, pp. 527-535, 2004.

[14] J. H. Chang, N. C. Hogan, and I. W. Hunter, "Needle-free interstitial fluid acquisition using a Lorentz-force actuated jet injector," in *Engineering in Medicine and Biology Society (EMBC), 2013 35th Annual International Conference of the IEEE*, 2013, pp. 3491-3494.

[15] K. Comley and N. Fleck, "Deep penetration and liquid injection into adipose tissue," *Journal of Mechanics of Materials and Structures*, vol. 6, pp. 127-140, 2011.

Graphical abstract